JOURNAL OF VISUAL COMMUNICATION AND IMAGE REPRESENTATION
Vol. 6, No. 1, March, pp. 35–51, 1995

Conformal Mapping-Based Image Processing: Theory and Applications

GUILLERMO A. BARICCO

Facultad de Ciencias Exactas y Naturales, Universidad de Buenos Aires, Argentina; and Advanced Solutions Department, IBM Argentina

ALFREDO M. OLIVERO

Laboratoire de Génie Informatique, Institut Imag, Grenoble, France; and ESLAI, Escuela Superior Latino Americana de Informática, Argentina

EDUARDO J. RODRÍGUEZ

Advanced Solutions Department, IBM Argentina; ESLAI, Escuela Superior Latino Americana de Informática, Argentina; and Computer Science Department, IBM Almaden Research Center, San Jose, California

FELIX G. SAFAR

Advanced Solutions Department, IBM Argentina; and Facultad de Ciencias Exactas, Universidad Nacional de la Plata, Argentina

AND

JORGE L. C. SANZ

Advanced Solutions Department, IBM Argentina; and Coordinated Sciences Laboratory, University of Illinois at Urbana–Champaign, Urbana, Illinois

Received February 11, 1992; accepted September 15, 1993

In this paper several techniques for numerical conformal mapping are surveyed and their applications to the development of novel methods in shape analysis and image classification are discussed. One of these techniques, based on the Szegö kernel, is illustrated by examples comprising distance transform and face representation and recognition. A conformal mapping-based face representation is presented. This face representation technique combined with an eigenface-based method extends and improves the results obtained with other eigenface algorithms. © 1995 Academic Press, Inc.

1. INTRODUCTION

In this paper, several techniques for the numerical computation of the conformal transformation between an arbitrary (but generally closed and simply connected) region of the complex plane and a fixed domain (e.g., the unit circle) are surveyed. This work explores the potential capabilities of these mappings as a way of representing shapes obtained from a two-dimensional digital image. Conformal maps have been proposed as a model of image representation by the human brain [2]. Since conformal mappings are one-to-one, no information is lost, and their high non-linearity is expected to provide an easy way of distinguishing small differences between two such shapes. Furthermore, conformal maps preserve some essential features of visual information.

The next two sections will be devoted to the analysis and discussion of several computational techniques appearing in the literature. All of them rely on the *Riemann Mapping Theorem* [3], which guarantees the existence of a unique function f from a certain region onto the unit circle, provided that a few conditions on the values of f and its derivative at a certain fixed point z_0 are satisfied. The techniques analyzed are Symm's integral equation method [4–7], Schwarz–Christoffel's methods [8–12], Fornberg's method [13], and the Szegö integral equation [14–17].

In Section 4, some definitions related to conformal mapping are given. The way "relevant features" are preserved by the application of conformal maps is analyzed.

In Section 5, a conformal map application to "eigenfaces" (technique developed by Sirovich and Kirby [1]) is

1047-3203/95 $6.00

presented. The conformal map space as a uniform environment for face representation is also analyzed. Several new algorithms for face representation are shown, and a discussion of experimental results obtained with a face data base of more than 120 images is also reported.

2. NUMERICAL METHODS FOR CONFORMAL MAPPING

A "conformal mapping" of a domain D is any function f with continuous partial derivatives on D, such that the oriented angle formed by the tangent vectors of two intersecting paths on D is preserved in the image of D by f [18]. In particular, orthogonal paths, such as equipotential and field lines, in D are mapped to orthogonal paths in $f(D)$ (Fig. 1).

Every conformal mapping is a holomorphic function with non-zero derivatives. Besides its theoretical relevance, conformal mapping methods have been applied to the solution of 2D potential problems on conservative (temperature, electro-magnetic, gravitational, etc.) fields; to impedance/admittance charts in electrical engineering; and to cartography (Mercator projection, Gauss–Krüger representation, etc.). In [19], it has been applied to texture mapping in computer graphics.

In this section, three methods for numerical evaluation of a conformal mapping are reviewed.

2.1. *Symm's Integral Equation Methods*

A classical approach [4–7] to the computation of the conformal mapping $f(z)$ from an arbitrary simply connected domain D with smooth boundary ∂D onto the interior of the unit circle in the w-plane is given by the expression

$$w = f(z) = e^{\log(z-z_0)+\gamma(z,z_0)}, \tag{1}$$

where z_0 is the pre-image of the center of coordinates of the w-plane, $\gamma = g + ih$ is an analytic function, and

$$g(z) = -\log|z - z_0|, \quad z \in \partial D, \tag{2}$$

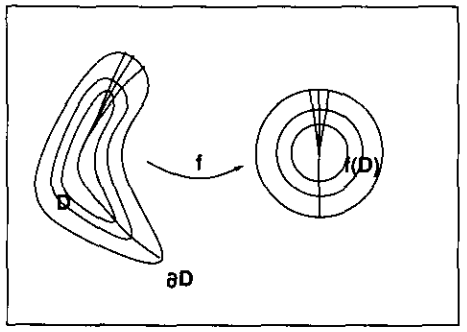

FIG. 1. Conformal mapping and orthogonal paths.

is the boundary condition. Setting z_0 equal to zero, the single-layer logarithmic potential representation of $g(z)$ becomes

$$g(z) = \int_{\partial D} \sigma(\zeta)\log|z - \zeta|\,|d\zeta|, \tag{3}$$

where $\sigma(\zeta)$ is the *source density*. Since $g(z)$ is continuous at the border, it follows from (2) and (3) that

$$\int_{\partial D}\sigma(\zeta)\log|z - \zeta|\,|d\zeta| = -\log|z|, \quad z \in \partial D. \tag{4}$$

To solve the integral equation (4), a suitable approximation to $\sigma(\zeta)$ must be provided.

In [6], the integration interval is partitioned into N subintervals, and a *ladder* model for σ is proposed. A better approximation is found in [5], where the interval is uniformly partitioned and an interpolating piecewise polynomial of degree 2, $\hat{\sigma}(s) = \sum_{i=1}^{N} P_i(s)\sigma_i$, is constructed.

In [7], an iterative scheme is proposed to calculate the coefficients t_k of the Fourier series expansion of $\sigma(u) = \sum_{k=-\infty}^{\infty} t_k e^{iku}$.

This method computes both the module and the argument of the mapping function and, due to unavoidable numerical errors, the uniform model is lost. Also, the main step of the outlined procedure (i.e., Eq. (4)) is a Fredholm integral equation of the first kind with a smooth kernel (wherever ζ does not belong to the interval of integration). The *ill-conditioning* of such equations is well known (see [20]). Nevertheless, in [5] the authors assume that the characteristics of the spectrum of the operator associated to the kernel will guarantee convergence. Neither a method for the computation of the mapping f for points in the interior of D nor one for the evaluation of the inverse $f^{(-1)}$ is given.

2.2. *Schwarz–Christoffel Methods*

The Schwarz–Christoffel (SC) formula maps the unit disk or the upper half-plane onto an arbitrary polygon with exterior angles β_k at the N corners w_k, developing a one-to-one correspondence f between the borders of these regions (supposed analytic in the open domain D and continuous at the boundary ∂D; see [3]).

Starting with the expression of the derivative of f,

$$\frac{df}{dz} = C\prod_{k=1}^{N}\left(1 - \frac{z}{z_k}\right)^{-\beta_k}, \tag{5}$$

it is easy to see that the image of the function f turns the right angles at the points z_k, $k = 1, \ldots, N$, which are called the *prevertices* and which satisfy $w_k = f(z_k)$ when the circle or the X axis is followed such that the region remains to the left of the curve. Integrating, the SC for-

mula is obtained:

$$w = w_c + C \int_0^z \prod_{j=1}^{N} \left(1 - \frac{\zeta}{z_j}\right)^{-\beta_j} d\zeta. \tag{6}$$

Nevertheless, further normalization conditions are needed to obtain a uniquely determined map. Two suitable choices would be to fix three of the boundary points z_k, or to fix one point z_1 and to let w_c be equal to an arbitrary location within the polygon.

The first numerical task is to find the values of the accessory parameters $z_1, \ldots, z_n$, C, and w_c that preserve the shape of the region. To do this computation, Trefethen suggests in [9] normalizing and formulating a nonlinear system of equations that provides the correct lengths of the sides of the image polygon.

As the integrand of the equation (6) is analytic, no problems arise.

For the evaluation of the inverse mapping two alternative procedures are proposed: the first is inverting (5), which leads to an ODE system, where any standard solver may be used; and the second is developing an iterative. Newton approximation using (6), where the w's are known.

In recent years, a number of extensions of the SC formula were presented. As a first example, the solution for circular arc polygons [10] should be mentioned. In [10], a differential equation involving first and second derivatives of the desired function—as well as the preimages of the vertices and the external angles of the polygon—is solved by the evaluation of the Taylor coefficients centered at the origin of the vertices, by means of adequate recurrence relations.

Also, the mapping of an annulus formed by two circles of radii ρ_1 and ρ_2 onto a given double-connected region is presented in [11]. In order to overcome the ill-conditioning of the standard SC transform for elongated regions, a new formula is introduced in [12] for the evaluation of the conformal mapping from an infinite strip parallel to the x-axis onto an arbitrary—possibly open—polygon. It remains to be analyzed if this approach does not lead to a severe scaling problem, due to the dispersion of the preimages of the vertices along the two lines that determine the strip.

Finally, a generalization of the method was introduced by Davis in [8]. Equation (5), which gives the map from the upper half-plane onto a polygon, is rewritten as

$$\frac{df}{dz} = Ce^{-\sum_{k=1}^{N}\beta_k \ln(1-z/z_k)}. \tag{7}$$

For a smooth border, differential elements may be considered; and in the limit, when $\beta(k)$ approaches $d\beta$ and z_k approaches ζ, an integral equation is obtained:

$$\frac{df}{dz} = Ce^{-\int \ln(1-z/\zeta)d\beta}. \tag{8}$$

The special case in which the boundary has corners can be included in (8). It suffices to treat β as a *step* function at the corners. Of course, the analytic expression for β is not known and must be guessed. The procedure suggested by Davis (which also fits the linear case) involves the piecewise-polynomial approximation of β and performing an iterative calculation of the parameter values under the assumption that the length of each side of the polygon is nearly proportional to the length of the corresponding segment of the real axis. At each step the values are updated using a quadrature of Eq. (8) that employs a modified trapezoidal rule. Once again it is seen that general formulas do not lead to easy calculations. Thus, unless a good model for the unknown variable is provided, less general methods are used.

2.3. *The Fornberg Method*

This method, presented by Fornberg [13], is based on the possibility of writing an analytic function as a Taylor series. The goal is then to find the Taylor coefficients (or a good approximation to them) that describe the Riemann function f (analytic) that conformally maps the unit circle onto a region D bounded by any smooth simply connected curve ∂D.

The idea is based on moving N points, ordered monotonically along the boundary curve ∂D, so that, through the unknown mapping f, they will come to correspond to the N roots of unity on the unit circle.

In [13], an iterative way to calculate an approximation of the Taylor coefficients and to find the boundary correspondence is presented. This method is general, in the sense that the mapping of all points of $\bar{D}$ (the closure of D) is calculated in the same form. Once the series coefficients are obtained, computing the function in any point reduces to the evaluation of the series.

A disadvantage of the method is that it requires information about the boundary curve and its first derivative for moving the points. Another problem is that the Taylor series may converge slowly, and truncation may produce large errors in the evaluation of the mapping.

3. THE SZEGÖ INTEGRAL EQUATION

3.1. *Introduction*

In this section, a technique based on the Szegö kernel will be reviewed. This method will be used for all the applications presented in this paper, thus special coverage will be devoted to this relatively recent technique for conformal maps.

Let D be a smooth, bounded, and simply connected domain. The Szegö kernel S [21] is associated with the

orthogonal projector onto the subspace of all square-integrable functions of the boundary ∂D that are boundaries of some holomorphic function of D. The Riemann mapping f from D onto the unit circle is related to S by the following two equations:

$$f'(z) = 2\pi \frac{S^2(z, a)}{S(a, a)}, \quad \text{for } z \in \overline{D}, \tag{9}$$

$$f(z) = \frac{1}{i} \dot{\gamma}(z) \frac{f'(z)}{|f'(z)|}, \quad \text{for } z \in \partial D, \tag{10}$$

where $\dot{\gamma}(z)$ is the unit vector tangent to ∂D at $z(t)$. The reason for the use of S is that it can be computed as the solution of a second-kind Fredholm integral equation, that is, a numerically stable problem.

3.2. *Description of the Method*

It is necessary to make some assumptions: ∂D is assumed to be twice continuously differentiable. Consequently, ∂D can be parameterized as $z(t)$, $0 \le t \le \beta$, with the property that $z(0) = z(\beta)$, $\dot{z}(0) = \dot{z}(\beta)$, $\ddot{z}(0) = \ddot{z}(\beta)$, with $\dot{z}(t) = dz/dt \neq 0$ for all t.

THEOREM 1 [15]. *$S(z, a)$ as a function of z is the unique solution of the integral equation*

$$h(z) + \int_{w \in \partial D} A(z, w) h(w) d\sigma_w = g(z), \quad z \in D, \tag{11}$$

where σ_w is the arc length on ∂D.

A is the Kerzman–Stein kernel [14], defined as

$$A(z, w) \overset{def}{=} \begin{cases} \overline{H}(z, w) - H(w, z), & w \in \partial D, z \in \partial D, w \neq z \\ 0, & w = z \in \partial D. \end{cases} \tag{12}$$

H is the Cauchy kernel, defined as

$$H(z, w) \overset{def}{=} \frac{1}{2\pi i} \frac{\dot{\gamma}(z)}{z - w}, \tag{13}$$

and g is defined as

$$g(z) \overset{def}{=} \overline{H(a, z)}. \tag{14}$$

Using another parameterization, the integral equation (11) becomes

$$\Upsilon(t) + \int_0^\beta k(t, s) \Upsilon(w) ds = \Omega(t), \quad 0 \le t \le \beta, \tag{15}$$

with

$$\Upsilon(t) = |\dot{z}(t)|^{1/2} h(z(t)), \tag{16}$$

$$\Omega(t) = |\dot{z}(t)|^{1/2} g(z(t)), \tag{17}$$

$$k(t, s) = |\dot{z}(t)|^{1/2} |\dot{z}(s)|^{1/2} A(z(t), z(s)). \tag{18}$$

The integral equation (15) can be solved using Nyström's method. Taking advantage of the periodicity of all the functions of Eq. (15), n equidistant collocation points $t_i = (i - 1)\beta/n$ and the trapezoidal rule for Nyström's method are chosen to obtain

$$\Upsilon(t_i) + \frac{\beta}{n} \sum_{j=1}^{n} k(t_i, t_j) \Upsilon(t_j) = \Omega(t_i), \quad 1 \le i \le n. \tag{19}$$

Defining the skew-Hermitian matrix B by

$$B_{ij} \overset{def}{=} \frac{\beta}{n} k(t_i, t_j) \tag{20}$$

and

$$\mathbf{x}_i = \Upsilon(t_i), \quad \mathbf{y}_i = \Omega(t_i), \tag{21}$$

the equation (19) can be rewritten as

$$(I + B)\mathbf{x} = \mathbf{y}. \tag{22}$$

The system of complex linear equations (22) can be solved by application of the Generalized Conjugate Gradient Method ([17] or Appendix B). By discretization of Eq. (15) the following *natural* interpolation formula is provided:

$$\Upsilon(t) = \Omega(t) - \frac{\beta}{n} \sum_{j=1}^{n} k(t, t_j) \Upsilon_j. \tag{23}$$

Unfortunately, Eq. (23) can be used only for the boundary, because $k(t_i, t_j)$ in the integral equation (15) is only defined on the boundary ∂D. This formula cannot be generalized to the interior of the region D. The Riemann mapping f can be written in terms of the boundary correspondence function $\theta(t)$ as

$$f(z(t)) = e^{i\theta(t)}. \tag{24}$$

Differentiating (24) yields

$$f'(z(t)) \dot{z}(t) = i e^{i\theta(t)} \dot{\theta}(t). \tag{25}$$

Using (9), (16), and (25), $\theta(t)$ is computed (without integration) using the following formula:

$$\theta(t) = \arg[-i\Omega^2(t) \dot{z}(t)]. \tag{26}$$

If the derivative $\dot{\theta}(t)$ is needed, taking absolute values in (25) yields

$$\dot{\theta}(t) = (2\pi/S(a, a))|\Omega^2(t)|. \tag{27}$$

The value of $S(a, a)$ can be calculated using the following formula [15]:

$$S(a, a) = \int_0^{\beta} |\Upsilon^2(t)|dt. \tag{28}$$

The inverse of the Riemann mapping function, $f^{(-1)}$, will be approximated by a polynomial of degree $m - 1$ ($m > n$). Details of the procedure are given in Appendix C.

3.3. *Discussion*

The importance of the Kerzman–Stein method resides in that it gives a way to calculate the mapping from an arbitrary region onto the unit circle (briefly, direct mapping) and information (without additional cost) for computing the inverse mapping.

Under the conditions of smoothness and boundedness for the domain D, and the twice differentiability of the boundary ∂D, the second-kind Fredholm equation (15) is guaranteed to be well-posed [20].

The convergence in solving the equation (22) by using the Conjugate Gradient Method is assured by the skew-hermitian property of the system's matrix.

The principal reasons that motivate the implementation of this method are that it can be applied to arbitrary regions, where other methods cannot be used, and the possibility of calculating the inverse mapping for specific applications.

Using Cauchy's theorem and the values of the function f in the border, it is possible to compute the value of f in the interior of the region.

3.4. *Algorithm*

Step 1. Extract samples of the border of the region. This may be done by application of a contour following algorithm, by an analytic expression of the curve, or in an interactive form.

Step 2. Fit the samples with B-splines, obtaining a parametrical description of the border.

Step 3. Choose N equally spaced collocation points $t_i = i/N$ for the parameter.

Step 4. Construct the matrix B_{ij} (Eq. (20)).

Step 5. Solve the system of the equation (22) by application of the Generalized Conjugate Gradient Method.

Step 6. Compute the value of $\theta(t)$ using the equation (26).

Step 7. If the inverse mapping is needed, follow the steps of Appendix C.

Step 8. Compute the value of the function f in the interior of the region by application of Cauchy's theorem.

The mapping obtained by the application of this method was compared with the analytic result for the mapping of some simple curves—i.e., ellipse, apple (epitrochoid), eccentric circle, etc. In this numerical test the error obtained was less than 0.3%. For the image size used (260 × 400), this error is negligible at a pixel level.

3.5. *Implementation Details*

The Szegö kernel method was implemented for the conformal mapping from an arbitrary region onto the unit circle.

An approximation of the region's boundary was obtained by using B-splines [Appendix A]. This representation assures the twice continuously differentiability of ∂D and gives a direct evaluation of the directions of the tangents in every point.

Taking advantage of the characteristics of the complex system of equations (the system's matrix is skew-hermitian), the resolution was done using the Conjugate Gradient Method [Appendix B], with the Orthomin variant. The method described in Section 3 was implemented for the computation of the inverse mapping.

All programs (B-spline fitting, Conjugate Gradient Method for complex systems, Szegö integral equation solution, eigenfaces decomposition (see Sections 4 and 5), and tools for image manipulation) were written in "C" on the AIX system running on a RISC System/6000 and X-windows tools were used to display the results.

4. APPLICATIONS TO IMAGE PROCESSING

4.1. *Definitions*

Conformal Transformation. Let D be a region of the z-plane and let f: $z \to w = f(z)$ be a conformal map of D onto a region E of the w-plane, with $z = x + iy$ and $w = u + iv$. The coordinates of the z-plane and of the w-plane are related by

$$\begin{cases} u = u(x, y) \\ v = v(x, y) \end{cases} \quad \text{or} \quad \begin{cases} x = x(u, v) \\ y = y(u, v). \end{cases} \tag{29}$$

Let a real-valued function ϕ: $(x, y) \to \phi(x, y) = \phi(z)$ be defined in D. A function ψ may then be defined in E as follows: for any $w \in E$,

$$\psi(w) := \phi(f^{(-1)}(w)) = \phi(x(u, v), y(u, v)). \tag{30}$$

Thus the value of ψ at w is equal to ϕ at the pre-image of w under the map f. The function ψ is called a *conformal transformation* of ϕ under the mapping f. It also holds

that

$$\phi(x, y) = \psi(u(x, y), v(x, y)). \tag{31}$$

The *complex gradient* of ϕ is the complex function

$$\nabla\phi\colon (x, y) \to \frac{\partial\phi}{\partial x}(x, y) + i\frac{\partial\phi}{\partial y}(x, y). \tag{32}$$

The *Laplacian* of ϕ is the real-valued function

$$\nabla^2\phi\colon (x, y) \to \frac{\partial^2\phi}{\partial x^2}(x, y) + \frac{\partial^2\phi}{\partial y^2}(x, y). \tag{33}$$

4.2. *Distance Transform*

Consider a digital binary image. A *distance transform* is an operation that converts this binary image to a gray-level image where all pixels have a value corresponding to the distance to the nearest boundary pixel [22].

For testing the application of conformal transformation to images, the distance transform of a digital image is taken as the function ϕ. Figure 2A shows the distance transform of a character and its conformal transformation. Note that the character structure and the angles between curves are preserved.

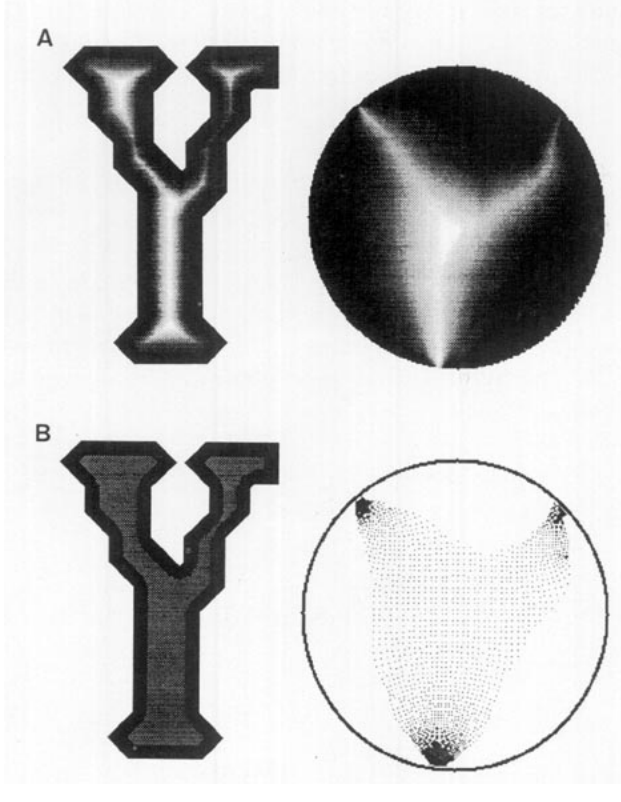

FIG. 2. (A) Distance transform of an image and its conformal transformation. (B) The point density variation for the conformal mapping.

4.3. *Preservation of "Relevant Features"*

Some of the most relevant features associated with the appearance of an image are its intensity edges. Classical methods for detecting edges in an image are based on gradient operators [23, pp. 351–353]. Estimators for the gradient functions work best when the gray-level transitions are abrupt, like those of a step function. One frequently encountered operator is the Laplacian operator, defined as in Subsection 4.1. A well-known edge detection is given by the position of the zero-crossings of the Laplacian of the image. Since the conformal transformation does not change the sign of the Laplacian (see Theorem 1 below), then its zero-crossings are preserved. Furthermore, since the conformal map preserves angles, the conformal transformation of an image will show the same structure of zero-crossings as the original image.

THEOREM 1 [3]. *If ψ results from ϕ by conformal transformation by means of the mapping $w = f(z)$, then*

$$\nabla_z^2\phi = \nabla_w^2\psi|f'|^2, \tag{34}$$

and thus

$$\operatorname{sgn}(\nabla_z^2\phi) = \operatorname{sgn}(\nabla_w^2\psi). \tag{35}$$

The proof is given in Appendix D.

4.4. *Variation of the Point Density in the Unit-Circle*

When an image is conformally transformed, its point density changes. This variation is produced by the high non-linearity of conformal mapping.

A clustering of points appears in the regions where elongations are mapped. The inverse effect (a dispersion of the points) occurs for the points that are close to the point that is mapped onto the origin. These characteristics are shown in Fig. 2B.

This phenomenon may produce numerical instabilities in the calculation of the conformal mapping for very elongated regions.

5. APPLICATION TO FACE REPRESENTATION AND RECOGNITION

5.1. *Face Representation*

The conformal transformation of a face image can be used as a representation technique. It is first necessary to define a simply closed curve that will be the border of the region to be mapped. This curve can enclose the whole face or a portion of it, depending on the application. Another possibility is that the curve can be the original face outline. The choice of the face outline is not acceptable as conformal maps are very sensitive to small perturbations in the boundary of regions.

The selected curve will be mapped onto the unit circle

boundary. By fixing the value of the map and its derivative at a point in the region, the mapping is uniquely determined.

As the conformal mapping is a one-to-one transformation, there exists an inverse mapping from the circle onto the region. By using this inverse, the original face can be reconstructed without loss of information.

The advantages of this representation are:

- Invariance to rotations, translations, and scale changes in the original domain and preservation of oriented angles and edge structure (Section 4).
- All faces are mapped onto the same region (the unit circle), thus yielding a uniform environment for better discrimination among different faces.
- With ellipses enclosing the face to be mapped it is possible to map some interesting points (for example, the pupils of the eyes) onto fixed points on the unit circle. This space warping is very important whenever the representation is used for recognition, because all the mapped images will have the critical areas for image recognition purposes mapped to the same location on the unit circle. Thus, the focus of attention and discrimination analysis can be concentrated in specific regions.

Compared to other space warping techniques, the conformal mapping is the only representation scheme that verifies all the above properties. As existing alternatives, [24] proposes the mapping $(x, y) \rightarrow (u(x, y), v(x, y))$, where u and v are harmonic functions. The book by Li *et al.* [25] presents several other transformations (bilinear, affine, perspective, etc.).

5.2. *Face Recognition Techniques*

There are in general two approaches to the problem of machine recognition of human faces.

1. The classical pattern recognition approach, consisting of two basic steps: feature extraction and classification. The success of such systems is dependent on the assumption that the information chosen is adequate for the task. There is an implicit dimensionality reduction in the representation by using features, making this approach computationally attractive. Several systems have been tried with different levels of success [26]. Perhaps the most impressive is that tried by Harmon *et al.* [27, 28]. It worked with high contrast photographs of face profiles, which were geometrically encoded. It achieved nearly perfect identification with a population of over 100 subjects. Other implementations make use of 2-D information [29] (use of deformable templates in the front view) and even 3-D shape [30].

However, it seems that individual features and their relationships comprise an insufficient representation to account for the performance of adult human face identification.

2. Global comparison of face images, in which approach the feature selection step is bypassed. No a priori judgement about the importance of face features is made. Instead, such systems try to characterize and encode variations among faces. They work with the pixel intensities of the digitized images previously put into a workable form. This approach to face recognition seeks to capture the configurational properties of a face, being more in accordance with the process of face recognition by humans. One of the main examples of systems for global comparison is the "eigenface" approach by Sirovich *et al.* [1], continued by Turk *et al.* [31], which captures the variation in a collection of face images, independent of any judgement of features. The idea is to decompose face images into linear combinations of a small set of characteristic images (eigenfaces added to the average face). This is done by diagonalizing the covariance matrix which characterizes the variation among faces. The pattern vector is formed by the coefficients of the "eigenface" expansion of a face. This information-theoretic approach to face representation opens a new avenue of research on face recognition.

5.2.1. Eigenfaces formulation. Each digitized image Φ is represented as a matrix Φ_{ij} of gray level values. It is convenient to regard the matrix Φ_{ij} as a vector φ (concatenation of matrix rows). An ensemble of digitized face images φ_n, $n = 1, \ldots, M$, is considered. The average face, for this ensemble, is calculated as

$$\bar{\varphi} = \frac{1}{M} \sum_{n=1}^{M} \varphi_n. \tag{36}$$

The deviation of φ_n with respect to the average face is

$$F_n = \varphi_n - \bar{\varphi}. \tag{37}$$

In [1], F_n is referred as a *caricature* of the face φ_n. The dimension D of the space is huge—close to 10^5 (260×400 pixels).

In [1], an optimal representation of the ensemble of caricatures is presented. It is based on a system of orthonormal vectors u_n, so that

$$(u_n, u_m) = \delta_{nm} \tag{38}$$

under the usual Euclidian inner product, with u_m calculated as

$$u_m = \sum_{k=1}^{M} \alpha_{mk} F_k. \tag{39}$$

The $\alpha_m = [\alpha_{mk}]_{k=1}^{M}$ are the eigenvectors of the matrix L; i.e.,

$$L\alpha_m = \lambda\alpha_m, \tag{40}$$

where

$$L_{mn} = (F_m, F_n). \tag{41}$$

L is a nonnegative symmetric matrix of dimension $M \times M$ ($M \ll D$).

This procedure for u_m calculation (40) results from the application of linear algebra methods to solve another related problem, i.e., finding the eigenvectors of the caricatures correlation matrix C ($D \times D$). This matrix is defined as

$$C = \frac{1}{M}\sum_{n=1}^{M} \langle F_n, F_n \rangle, \tag{42}$$

where $\langle F_n, F_n \rangle = F_n \cdot F_n^T$. The matrix C is symmetric and nonnegative, and its eigenvalues and orthonormal eigenvectors are just

$$Cu_n = \lambda_n u_n, \tag{43}$$

providing the same solution as that obtained by the low-dimensional approach. The numerical resolution of this original problem, however, is an intractable task. This alternative view of the problem is connected with the Karhunen–Loève expansion [1].

Remark. A detailed analysis of the conditions under which the equation (40) is obtained shows that the matrix $K = [F_1 \ldots F_M]$ must have a pseudo-inverse. This point is not mentioned in the literature, and without this condition the eigenvectors which were calculated based on (40) are different than those calculated by solving (43). A simple way to overcome this problem is by calculating the average face $\bar{\varphi}$ with some additional faces out of the ensemble, making the set of F_i vectors linearly independent.

5.3. *Eigenfaces and Conformal Mapping*

The Eigenfaces Method, as described previously, has some weak points. Even avoiding scaling and taking images under controlled conditions, the process of averaging face images suffers from mismatch problems (e.g., the eyebrow of one image is superimposed and averaged with the eye of another image, and so on). The resulting face becomes extremely blurred, with a lack of detail.

As a result, the caricature or *error image* F keeps almost all the information of the original face. Therefore, when applying eigen-decomposition to the *error image* F, much of the representation power is spent in just restoring basic features (common to all faces) only partially included in the average face, rather than describing the distinctive details of a particular face. This results in the requirement of a considerably large number of terms when small representation errors are sought.

The eigenvector representation would become much more efficient if the regions of interest were forced to coincide somehow. Conformal mapping can be fruitfully used for this purpose. By pre-warping the face images, relevant areas (eyes, mouth, nose, etc.) can be made to coincide on the unit circle. Eigenanalysis can then be performed on this uniform domain. In particular, the resulting average image on the unit disc keeps most of the common face features, leaving the error images to better characterize among individuals.

5.4. *Experimental Procedures and Results*

In order to carry out the experimental work more than 120 faces were taken. Individuals were drawn from both male and female populations (65% men, 35% women). In the construction of the data base no special selection procedure (sex, race, etc.) was used. Each face was digitized at 360 × 480 pixels with 64 gray level by means of an IBM Video Capture Adapter and Audio Visual Connection software. All images were processed by changing the format, the dimensions (260 × 400), and the gray-level range (0–255). A vertical line passed through the symmetry line of the face and a horizontal line through the pupils of the eyes, just to aid in the alignment of the image. No other conditions (like background lighting or field depth) were enforced.

Two eigenface-based representation methods were compared. One method is the classical eigenface technique based on eigenanalysis carried out in the image domain [31]. The second method is the new technique based on eigenanalysis carried out on the unit disc. The conformal map chosen is the one that realizes the conditions expressed in Fig. 3A, i.e., the five distinguished points map onto *fixed* points on the unit circle. In order to obtain this, two maps need to be done, in which the curve selected for defining each mapping is an ellipse.

One ellipse was chosen so that its center maps to the center of the circle, and the axes are such that the pupil centers map onto two fixed points on the unit circle. The second ellipse was used to map the corners of the mouth onto fixed points on the lower half of the unit circle. See Fig. 3A.

The final map is done by combining the top half of the first map with the bottom half of the second map, as shown in Fig. 4.

For determining the ellipses' axes, so that the points of interest (in this case the eye centers and the corners of the mouth) are mapped onto the fixed points on the unit circle, the following procedure was used.

Step 1. Fix a point p inside the unit circle C where a distinguished point q of the original image has to

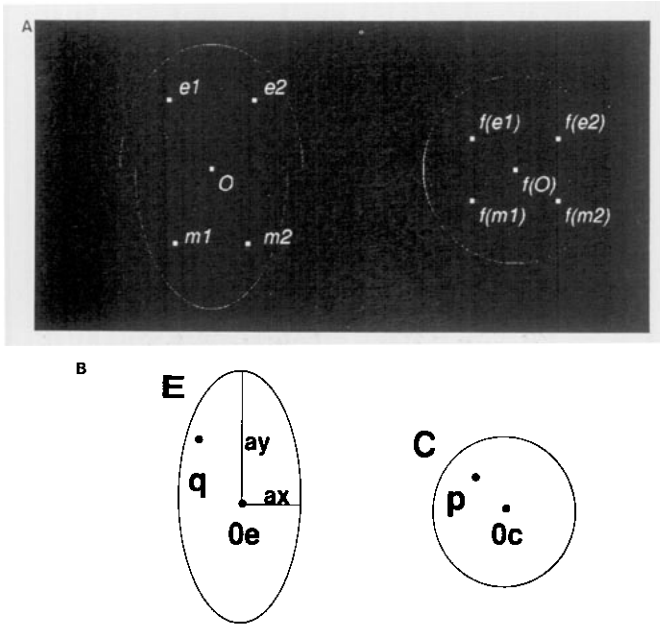

FIG. 3. (A) The five distinguished points map onto fixed points on the unit circle. (B) Parameters used for selecting the boundary ellipse.

be mapped for all images in the face data base (Fig. 3B).

Step 2. Repeat for different values of ax, ay.
  Step 2.1. Select the axes a_x, a_y of the ellipse E.
  Step 2.2. Compute the conformal mapping f so that E is mapped onto C and $f(0_E) = 0_C$.
  Step 2.3. Compute $q = f^{-1}(p)$.

Step 3. Make a table with all q, ax, and ay obtained in Step 2.

Step 4. Repeat for all faces in the face data base.
  Step 4.1. Given a face, determine the center of the eyes (or the corners of the mouth). This step is done manually over the face data base at the present time.
  Step 4.2. Find in the table the closest q to the point determined in Step 4. Take ax and ay as the chosen axes of the ellipse.

The same procedure was used for e_2, m_1, m_2 (Fig. 3A).

It is important to note that the selection of ellipses as face-enclosing curves precludes the numerical instability mentioned earlier (Section 4.4), as long as they are only moderately elongated (aspect ratio close to one).

One of the most relevant results is related to the average face: using conformal transformation, the average face appearance (in human visualization) is much clearer than the appearance without using conformal transformation. This happens because more information about the ensemble of faces is contained in the average image computed on the unit disc.

The average faces with and without conformal mapping pre-processing are shown in Fig. 5. Part A corresponds to the average of the original faces and part B corresponds to the average of the conformal deformed faces. Figures 6 and 7 show a subset of the corresponding eigenfaces for both methods.

The most important result is that, for face identification by humans, fewer eigenfaces are needed with conformal

FIG. 4. The original face and the final map.

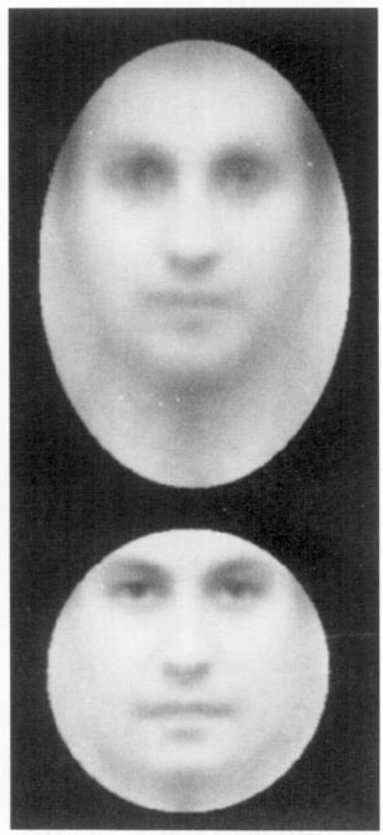

FIG. 5. Average faces: Original (top) and with conformal map (bottom).

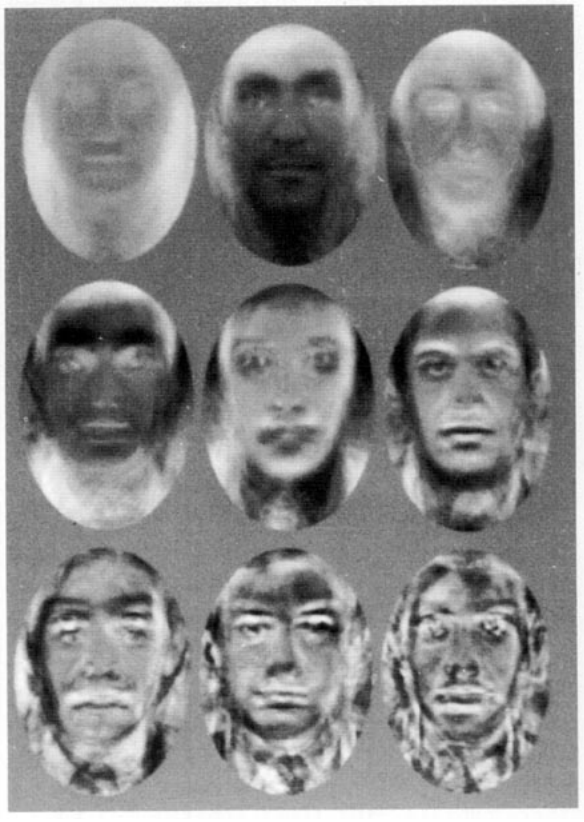

FIG. 6. A subset of eigenfaces for original faces data base.

transformation than without conformal transformation (Fig. 8).

Let F be a face and $a_n = \langle F, u_n \rangle$ its coefficients in the eigenface base; the partial face reconstruction for F is

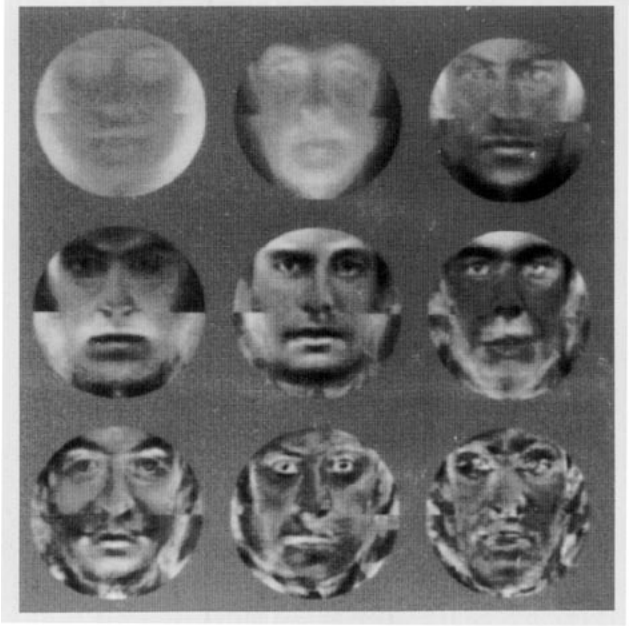

FIG. 7. A subset of eigenfaces for conformal faces data base.

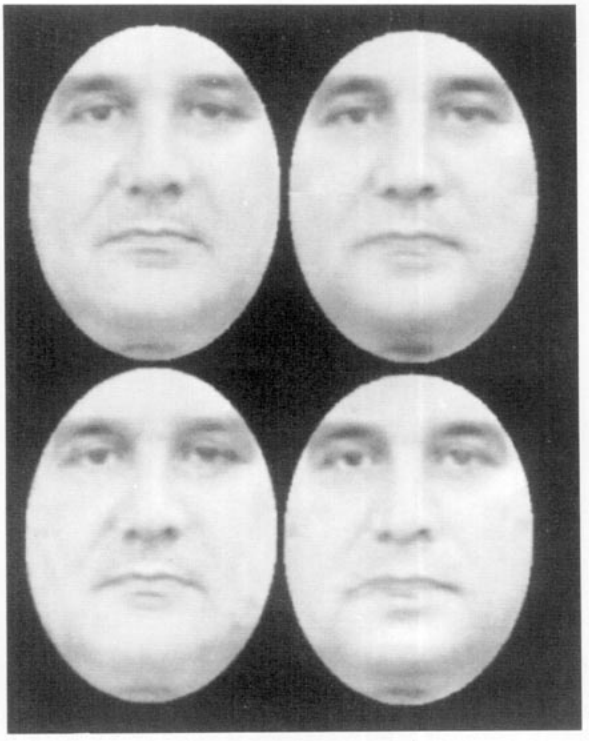

FIG. 8. Partial reconstruction using different methods.

defined as

$$F^N = \bar{\varphi} + \sum_{n=1}^{N} a_n * u_n, \tag{44}$$

where

$$F = F^M. \tag{45}$$

Two type of experiments were made. Each face was reconstructed first, using the coefficients in the original order of the eigenvectors (corresponding to a descending order of the eigenvalues) and second using the coefficients ordered by the descending order of their absolute values.

In the first case the number of eigenfaces required for human recognition of the reconstruction in the proposed method was "50" compared to "65" for the original eigenface method [31]. In the other experiment, the number of eigenfaces were "20" and "40," respectively. See Fig. 8. Comparisons were made between the faces reconstructed by the original eigenface method and those reconstructed by the combination of conformal transformation, eigenface reconstruction, and inverse conformal transformation. Figures 9–12 show reconstruction of one face using 1, 10, 20, 30, 40, 50, 60, 70, 80, and 85 eigenfaces. Note the improved and smoother reconstruction in

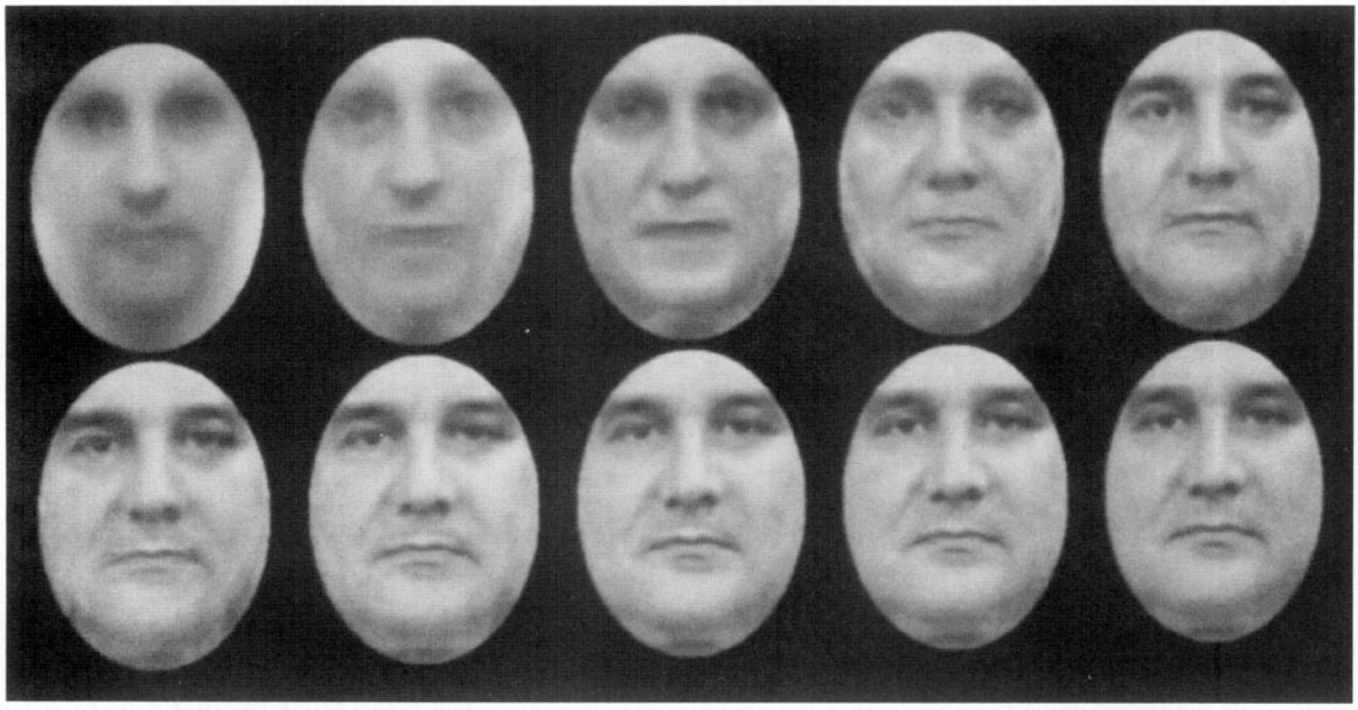

FIG. 9. Reconstruction of one face with the original method using 1, 10, 20, 30, 40, 50, 60, 70, 80, and 85 eigenfaces.

the conformal mapped case, also free from the artifacts observed in the non-mapped representation. Only in the former case can partial reconstructions be enhanced by using standard image processing techniques, e.g., high-pass filtering, with no artifact amplification.

The error or measure of goodness in the reconstruction was calculated as

$$e_N = \frac{\|F - F^N\|}{\|F\|}, \tag{46}$$

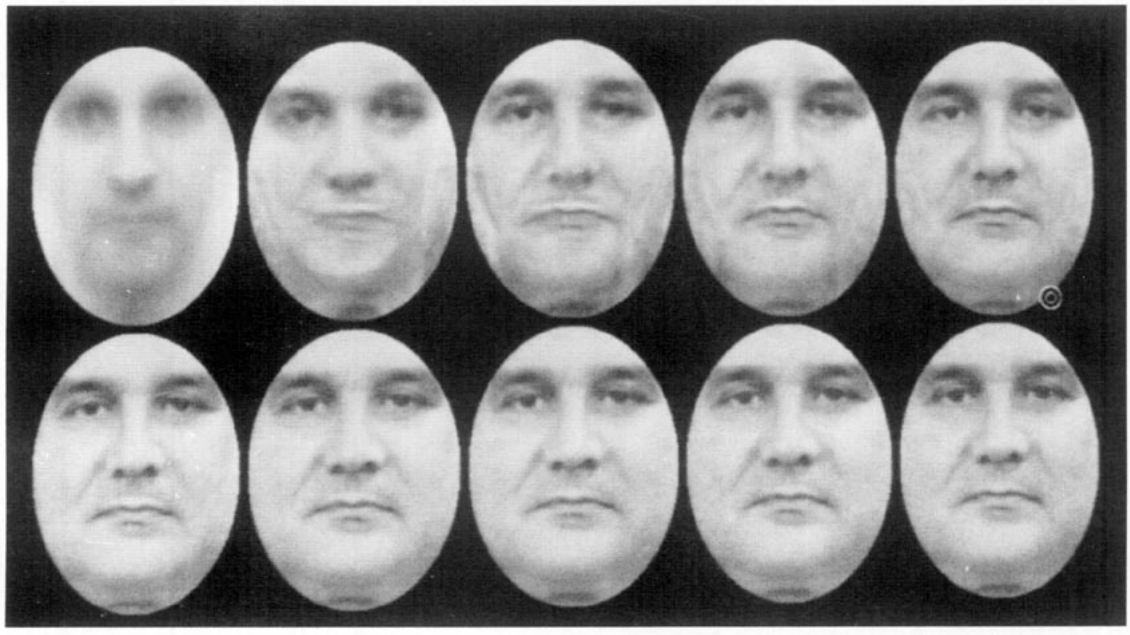

FIG. 10. Reconstruction of one face with the original method (coefficient sorted) using 1, 10, 20, 30, 40, 50, 60, 70, 80, and 85 eigenfaces.

FIG. 11. Reconstruction of a face with the conformal method using 1, 10, 20, 30, 40, 50, 60, 70, 80, and 85 eigenfaces.

where

$$\|F\| = \sum_{n=1}^{M} |F_n|. \tag{47}$$

The mean of the error of the reconstruction for both methods was calculated over the data base set, resulting in less error for the faces that were preprocessed using conformal mapping. Figure 13 shows these average errors as a function of the number of eigenfaces used in the reconstruction. Figure 14 shows the error in the reconstructions corresponding to the face in Fig. 4.

The accumulated energy in the first N coefficients of a face is defined as

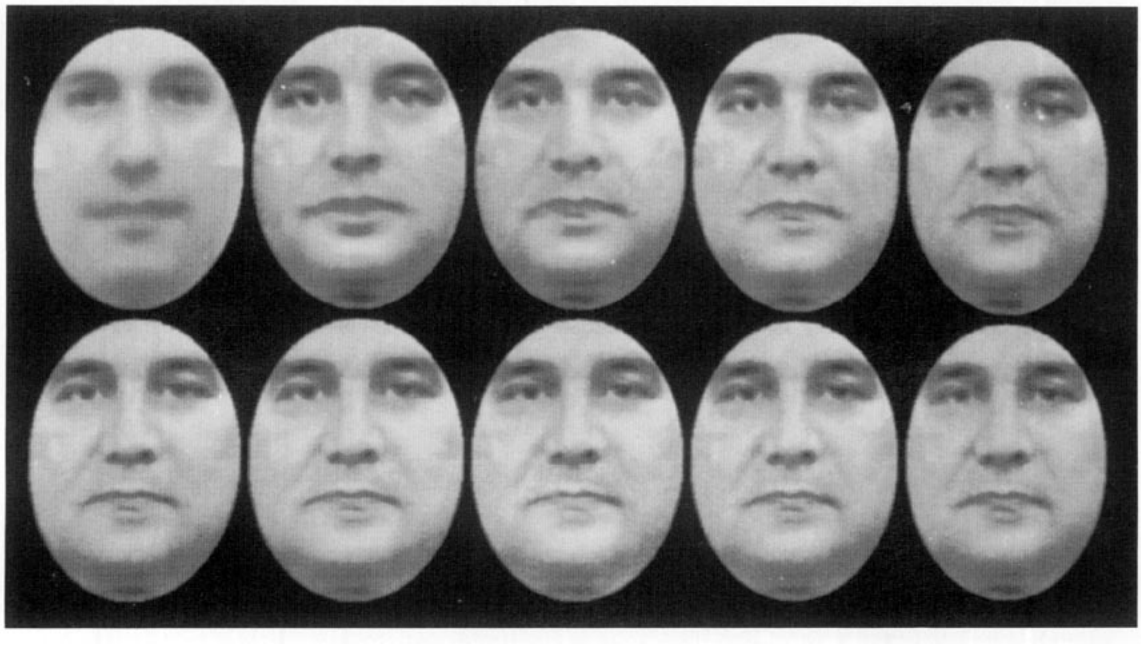

FIG. 12. Reconstruction of a face with the conformal method (sorted coefficients) using 1, 10, 20, 30, 40, 50, 60, 70, 80, and 85 eigenfaces.

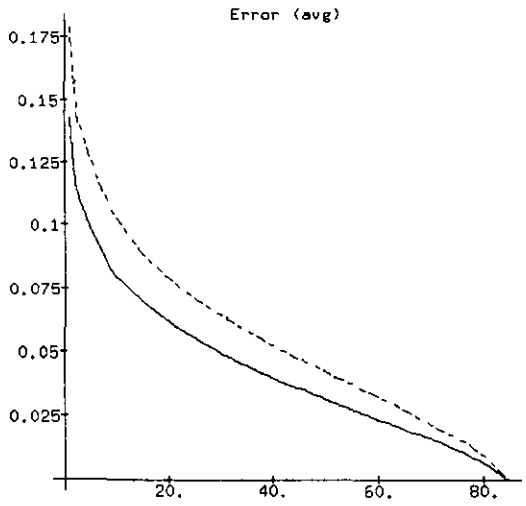

FIG. 13. Average error vs number of the eigenfaces used in the reconstruction.

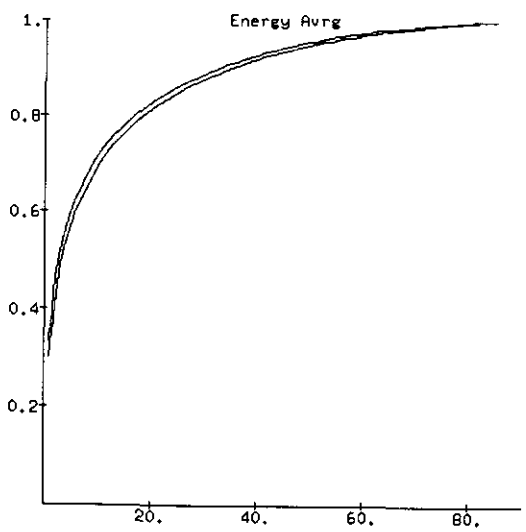

FIG. 15. The mean of the accumulated energy vs number of coefficients.

$$E_N = \sum_{n=1}^{N} |a_n|^2. \tag{48}$$

The mean of the accumulated energy as a function of the number of coefficients was calculated for both techniques (Fig. 15). Currently, different metrics for the recognition process are being studied.

In short, the face representation technique presented here extends and improves the results obtained with eigenface algorithms.

6. CONCLUSIONS

A survey of techniques for numerical conformal mapping is presented along with some applications to image processing. Conformal transforms provide a representation mechanism in which different shapes can be mapped onto a single domain, the unit circle. A conformal image transformation preserves key features such as the zero-crossings of the Laplacian.

The Kerzman–Stein method was implemented and explored in detail as a powerful technique for computing direct and inverse mappings between a region of arbitrary shape and the unit circle. This mathematical transform was used to compute conformal maps for binary and gray-level images.

Finally, a novel conformal mapping-based face representation was presented. Based on eigenanalysis of warped face images on the unit circle, this representation results in better reconstructions than those obtained with other eigenface methods. By keeping the most common face information in a warped face average in the unit circle, the resulting eigenfaces provided better representations of the variations among individuals. This result was validated by extensive experimentation over a medium-sized database of faces.

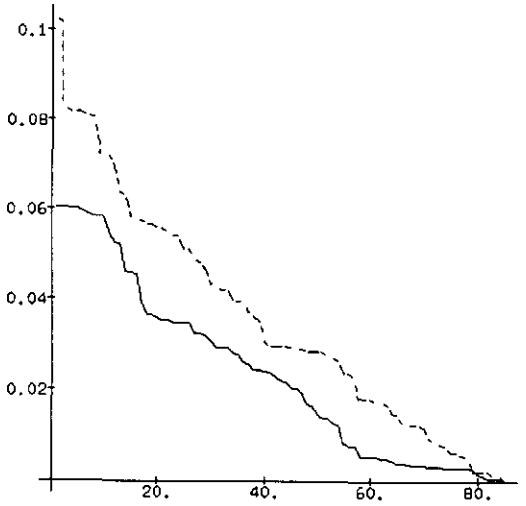

FIG. 14. Error in the reconstruction of face of Fig. 4 vs number of the eigenfaces used in the reconstruction.

APPENDIX A: B-SPLINE FITTING

In several tasks in image processing, one has to approximate the shapes of objects appearing in digital pictures. It is often important and useful to have an analytic model that comprises the relevant information of the boundary of the shapes. The model to be chosen should be a suitable parameterization of a closed planar curve providing the best fit to the set of boundary pixels under certain criteria. A common criterion involves the minimization of the Euclidean distance between the model and the points, that is, the *least squares approximation*. This

fitting is preferred upon an interpolating scheme because of its lower dependence on boundary noise fluctuation due to the sampling and binarization processes [33].

A powerful enough tool for fitting purposes is the B-spline form of periodic piecewise polynomials of a certain fixed degree d. Normalized B-splines are themselves periodic piecewise polynomials, and they are defined by the well-known relationship [34]

$$N_{i,1}(u) = \begin{cases} 1, & t_i \le u \le t_{i+1} \\ 0, & \text{otherwise} \end{cases} \tag{49a}$$

$$N_{i,r}(u) = \frac{(u - t_i)N_{i,r-1}(u)}{t_{i+r-1} - t_i} + \frac{(t_{i+r} - u)N_{i+1,r-1}(u)}{t_{i+r} - t_{i+1}}, \quad r = 2, \ldots, d, \tag{49b}$$

for $i = 0, \ldots, n-1$, $t_0 \le u \le t_n$, given the sequence $K = [t_0, \ldots, t_n]$ of parameter values called the *knots* that correspond to the junction of two polynomial pieces. This definition holds in the interval $t_0 \le u \le t_n$, assuming that the knots t_i have a periodic numbering. In order to obtain a function defined over the whole real line, the parameter u is evaluated module $t_n - t_0$. In this way, if the inequalities are strict, $N_{i,d} \in C^{d-1}$. Any C^{d-1} periodic piecewise polynomial P of degree d over K (or *spline* for brevity) may be represented as a linear combination of the normalized B-splines of the same degree, defined by the same knot sequence, since they constitute a basis for the subspace of these *splines*,

$$\mathbf{P}(u) = \sum_{i=0}^{n-1} \mathbf{c}(i)N_{i,r}(i). \tag{50}$$

The weights $\mathbf{c}$ are 2-D vectors when just planar curves are being considered, and may be understood as points of $\mathcal{R}^2$ that locally control the shape of the curve being modeled. They shall be referred to as *control points*. Given a set of boundary pixels that may be considered as samples of the continuous function $\hat{P}$, for a sequence $[u_0, \ldots, u_{m-1}]$ of values of the parameter

$$P_i = \hat{P}(u_i), \quad i = 0, \ldots, m-1, \tag{51}$$

the following matrix equation summarizes the least-squares problem to be solved

$$\hat{P} = \mathbf{HC}, \tag{52}$$

where $\hat{P} = [\hat{x}, \hat{y}]$ is the $m \times 2$ data matrix, $C = [C_x, C_y]$ is the $n \times 2$ control points matrix, and $H = N_{j,r}(u_i)$, $i = 0 \ldots m-1, j = 0 \ldots n-1$, is the $m \times n$ matrix of the normalized B-splines evaluated on the data points. The least-squares approximation is obtained, solving the so-called *normal equations*

$$H^t\hat{P} = H^t HC. \tag{53}$$

This is a non-singular square system of linear equations, and it can be solved by any of the well-known methods, profiting from the Toeplitz structure of H^tH. The elements of H are computed using the recurrence relation (49) for the value u_i of the parameter.

APPENDIX B: VARIATIONAL ITERATIVE METHODS FOR LINEAR SYSTEM SOLVING

B.1. *Introduction*

A useful tool for solving large systems of linear equations is given by iterative methods. One characteristic of these methods is that they start with an initial solution, and in each iteration they build a new approximation. The sequence of approximations converges, under certain conditions, to a solution of the linear problem.

One of these methods is the conjugate gradient method (CG). This method, presented by Stiefel, is used to approximate the solution of system of linear equations

$$Ax = f. \tag{54}$$

Applying CG to a real, symmetric, and positive-definite $N \times N$ matrix, an exact solution, in the absence of round-off errors, is obtained in at most N steps. This method gives a good approximation of the solution of the linear system in a few steps.

One generalization (GCG) of the method was introduced by Eisenstat *et al.* [35] for non-symmetric systems. Like CG, GCG gives the solution in at most N steps.

B.2. *Variations of GCG*

The GCG presents some variations according to how the next direction is calculated. All methods have the same general form:

(2.1) Choose x_0
(2.2) Compute $r_0 = f - Ax_0$
(2.3) Set $p_0 = r_0$
For $i = 0$ **Step 1 Until** *Convergence* **Do**
(2.4) $a_i = (r_i, Ax_i)/(Ap_i, Ap_i)$
(2.5) $x_{i+1} = x_i + Ap_i$
(2.6) $r_{i+1} = r_i - a_iAp_i$
(2.7) Compute p_i

The choice of a_i in (2.4) minimizes $\|r_{i+1}\|_2 = \|f - A(x_i + ap_i)\|_2$ as a function of a, so that the norm of the residual decreases in each step. The variations of the GCG differ in the technique used to compute the new p_{i+1}.

B.2.1. Conjugate Residual Method (CR). For this method, p_{i+1} is calculated as

$$p_{i+1} = r_{i+1} = b_i p_i \tag{55}$$

with

$$b_i = -\frac{(Ar_{i+1}, Ap_i)}{(Ap_i, Ap_i)}. \tag{56}$$

B.2.2. Generalized Conjugate Residual Method (GCR). The CR can be generalized using all the previous directions to calculate p_{i+1},

$$p_{i+1} = r_{i+1} + \sum_{j=0}^{i} b_j^{(i)} p_j \tag{57}$$

with

$$b_j^{(i)} = -\frac{(Ar_{i+1}, Ap_j)}{(Ap_j, Ap_j)}, \quad j \le i. \tag{58}$$

B.2.3. Orthomin(k). The GCR method has high work and storage requirements for a large N. A variant to GCR is to use only the k previous directions. This variant receives the name Orthomin(k). Then p_{i+1} is calculated as

$$p_{i+1} = r_{i+1} + \sum_{j=i-k+1}^{i} b_j^{(i)} p_j \tag{59}$$

with $b_j^{(i)}$ as in GCR.

B.2.4. GCR(k). Another modification to the GCR method is to restart it periodically (each $k + 1$ iterations). The current value of $x_{j(k+1)}$ is used as the new starting guess. This method is called GCR(k).

B.2.5. Minimum Residual Method (MR). When $k = 0$, Orthomin(k) and GCR(k) are identical. In this particular case the method is called the Minimum Residual Method.

$$p_{i+1} = r_{i+1} \tag{60}$$

APPENDIX C: COMPUTING THE INVERSE MAPPING

The procedure described in this appendix [15] is based on the approximation of $f^{(-1)}$, by g, a $(m - 1)$-degree polynomial $(m > n)$:

$$g(w) = \sum_{j=0}^{m-1} \xi_j w^j. \tag{61}$$

Step 1. Define m equidistant points on the unit circle, at angles $\theta_j = 2\pi j/m$.

Step 2. Compute the parameter values $\tau_j = \theta^{(-1)}(\theta_j)$, using Newton's method,

$$\tau_j^{(k+1)} = \tau_j^{(k)} + \frac{\theta_j - \theta(\tau_j^{(k)})}{\dot{\theta}(\tau_j^{(k)})}, \tag{62}$$

where $\dot{\theta}(\tau_j^{(k)})$ is provided as a byproduct when the direct map is calculated (Eq. 27).

Step 3. Obtain the pre-images of the equidistant points on the unit circle:

$$z(t_j) = z_j = f^{(-1)}(e^{2\pi ij/m}). \tag{63}$$

Step 4. Compute the coefficients ξ_j such that g interpolates $f^{(-1)}$ at the points $e^{2\pi ij/m}$:

$$\xi_j = \frac{1}{2\pi}\int_0^{2\pi} g(e^{i\theta})e^{-ij\theta}\, d\theta. \tag{64}$$

This can be done by using the FFT in $m \log m$ operations [7].

APPENDIX D: RELATED THEOREMS

Proof of Theorem 1. By using the chain rule in the definition of the conformal transformation (31), it follows that

$$\frac{\partial \phi}{\partial x} = \frac{\partial \psi}{\partial u}\frac{\partial u}{\partial x} + \frac{\partial \psi}{\partial v}\frac{\partial v}{\partial x} \tag{65}$$

$$\frac{\partial \phi}{\partial y} = \frac{\partial \psi}{\partial u}\frac{\partial u}{\partial y} + \frac{\partial \psi}{\partial v}\frac{\partial v}{\partial y}. \tag{66}$$

By the Cauchy–Riemann equations,

$$\frac{\partial \phi}{\partial y} = -\frac{\partial \psi}{\partial u}\frac{\partial v}{\partial x} + \frac{\partial \psi}{\partial v}\frac{\partial u}{\partial x}. \tag{67}$$

From (65) and (66), using the chain rule repeatedly, we get

$$\frac{\partial^2 \phi}{\partial x^2} = \frac{\partial^2 \psi}{\partial u^2}\left(\frac{\partial u}{\partial x}\right)^2 + \frac{\partial \psi}{\partial u}\frac{\partial^2 u}{\partial x^2} + \frac{\partial^2 \psi}{\partial v^2}\left(\frac{\partial v}{\partial x}\right)^2 + \frac{\partial \psi}{\partial v}\frac{\partial^2 v}{\partial x^2} + 2\frac{\partial^2 \psi}{\partial u \partial v}\frac{\partial u}{\partial x}\frac{\partial v}{\partial x} \tag{68}$$

and

$$\frac{\partial^2 \phi}{\partial y^2} = \frac{\partial^2 \psi}{\partial u^2}\left(\frac{\partial u}{\partial y}\right)^2 + \frac{\partial \psi}{\partial u}\frac{\partial^2 u}{\partial y^2} + \frac{\partial^2 \psi}{\partial v^2}\left(\frac{\partial v}{\partial y}\right)^2 + \frac{\partial \psi}{\partial v}\frac{\partial^2 v}{\partial y^2} + 2\frac{\partial^2 \psi}{\partial u \partial v}\frac{\partial u}{\partial y}\frac{\partial v}{\partial y}. \tag{69}$$

Thus, it follows that

$$\nabla^2\phi = \frac{\partial^2\psi}{\partial u^2}\left(\left(\frac{\partial u}{\partial x}\right)^2 + \left(\frac{\partial u}{\partial y}\right)^2\right) + \frac{\partial\psi}{\partial u}\left(\frac{\partial^2 u}{\partial x^2} + \frac{\partial^2 u}{\partial y^2}\right)$$
$$+ \frac{\partial^2\psi}{\partial v^2}\left(\left(\frac{\partial v}{\partial x}\right)^2 + \left(\frac{\partial v}{\partial y}\right)^2\right) + \frac{\partial\psi}{\partial v}\left(\frac{\partial^2 v}{\partial x^2} + \frac{\partial^2 v}{\partial y^2}\right)$$
$$+ 2\,\frac{\partial^2\psi}{\partial u\partial v}\left(\frac{\partial u}{\partial x} + \frac{\partial u}{\partial y}\frac{\partial v}{\partial y}\right).$$

By the Cauchy–Riemann equations,

$$\frac{\partial u}{\partial x}\frac{\partial v}{\partial x} + \frac{\partial u}{\partial y}\frac{\partial v}{\partial y} = 0 \tag{70}$$

and

$$\frac{\partial^2 u}{\partial x^2} + \frac{\partial^2 u}{\partial y^2} = \frac{\partial^2 v}{\partial x^2} + \frac{\partial^2 v}{\partial y^2} = 0. \tag{71}$$

Furthermore,

$$\left(\frac{\partial u}{\partial x}\right)^2 + \left(\frac{\partial u}{\partial y}\right)^2 = \left(\frac{\partial v}{\partial x}\right)^2 + \left(\frac{\partial v}{\partial y}\right)^2 = \left|\frac{\partial u}{\partial x} + i\frac{\partial v}{\partial x}\right|^2 = |f'(z)|^2. \tag{72}$$

Thus,

$$\nabla_z^2\phi = \nabla_w^2\psi|f'|^2 \tag{73}$$

and

$$\operatorname{sgn}(\nabla_z^2\phi) = \operatorname{sgn}(\nabla_w^2\psi). \quad \blacksquare$$

REFERENCES

1. L. Sirovich and M. Kirby, Low-dimensional procedure for the characterization of human faces, *J. Opt. Soc. Amer. A* **4**(3), 1987, 519–524.
2. C. F. Frederick and E. L. Schwartz, Conformal image warping, *IEEE Comput. Graphics Appl.* 1990, 54–61.
3. P. Henrici, *Applied and Computational Complex Analysis*, Vol. 1, Wiley, New York, 1974.
4. J. K. Hayes, D. K. Kahaner, and R. G. Kellner, An improved method for numerical conformal mapping, *Math. Comp.* **26,** 1972, 327–334.
5. J. K. Hayes, D. K. Kahaner, and R. G. Kellner, A numerical comparison of integral equations of the first and second kind for conformal mapping, *Math. Comp.* **29,** 1975, 512–521.
6. G. T. Symm, An integral equation method in conformal mapping, *Numer. Math.* **9,** 1966, 250–258.
7. P. Henrici, Fast Fourier methods in computational complex analysis, *SIAM Rev.* **21,** 1979, 481–527.
8. R. T. Davis, Numerical methods for coordinate generation based on Schwarz–Christoffel transformations, in *Proc. 4th Amer. Inst. Aero. Astro. Computational Fluid Dynamics Conference, Williamsburg, VA, 1979.*
9. L. N. Trefethen, Numerical computation of the Schwarz–Christoffel transformation, *SIAM J. Sci. Statist. Comput.* **1,** 1980, 82–102.
10. P. Bjørstad and E. Grosse, Conformal mapping of circular arc polygons, *SIAM J. Sci. Statis. Comput.* **8,** 1987, 19–32.
11. E. Hoekstra, Coordinate generation in symmetrical interior, exterior, or annular 2D domains, using a generalised Schwarz–Christoffel transformation, in *Numerical Grid Generation in Computational Fluid Dynamics, Proc. of the International Conference held at Landshut, W. Germany, 1986,* pp. 59–70.
12. L. H. Howell and L. N. Trefethen, A modified Schwarz–Christoffel transformation for elongated regions, *SIAM J. Sci. Statist. Comput.* **11,** 1990, 928–949.
13. B. Fornberg, A numerical method for conformal mappings, *SIAM J. Sci. Statist. Comput.* **1,** 1980, 386–400.
14. N. Kerzman and E. M. Stein, The Cauchy kernel, the Szegö kernel, and the Riemann mapping function, *Math. Ann.* **236,** 1978, 85–93.
15. N. Kerzman and M. R. Trummer, Numerical conformal mapping via the Szegö kernel, *J. Comp. Appl. Math.* **14,** 1986, 111–123.
16. S. T. O'Donnell and V. Rokhlin, A fast algorithm for the numerical evaluation of conformal mappings, *SIAM J. Sci. Statist. Comput.* **10,** 1989, 475–487.
17. M. R. Trummer, An efficient implementation of a conformal mapping method based on the Szegö kernel, *SIAM J. Numer. Anal.* **23,** 1986, 853–872.
18. R. V. Churchill, *Complex Variables and Applications,* 2nd ed., McGraw–Hill, New York, 1960.
19. E. Fiume, A. Fournier, and V. Canale, Conformal texture mapping, in *Proc. Eurographics '87, 1987,* pp. 53–64.
20. G. Dahlquist and Å. Björk, *Numerical Methods,* Prentice–Hall, Englewoods Cliffs, NJ, 1974.
21. P. Henrici, *Applied and Computational Complex Analysis,* Vol. 3, Wiley, New York, 1980.
22. G. Borgefors, Distance transformations in digital images, *Comput. Graphics Image Process.* **34,** 1986, 344–371.
23. A. K. Jain, *Fundamentals of Digital Image Processing,* Prentice–Hall, Englewoods Cliffs, NJ, 1989.
24. Z. C. Li, C. Y. Suen, T. D. Bui, and Q. L. Gu, Harmonic models of shape transformations in digital images and patterns, in *10th International Conference on Pattern Recognition, 1990,* Vol. 2, pp. 1–7.
25. Z. C. Li, T. D. Bui, Y. Y. Tang, and C. Y. Suen, *Computer Transformations in Digital Images and Patterns,* World Scientific, Singapore, 1989.
26. G. J. Kaufman and K. J. Breeding, The automatic recognition of human faces from profile silhouettes, *IEEE Trans. Systems, Man, Cybernetics* **6,** 1976, 113–121.
27. L. Harmon and W. Hunt, Automatic recognition of human face profiles, *Comput. Graphics Image Process.* **6,** 1977, 135–156.
28. L. D. Harmon, Lasch, and Ramig, Machine identification of human faces, *Pattern Recognition* **13,** 1981, 97–110.
29. A. L. Yuille, D. S. Cohen, and P. W. Hallinan, Feature extraction from faces using deformable templates, in *Proc. CVPR, San Diego, CA, 1989.*
30. J. T. Lapresté, J. Y. Cartoux, and M. Richetin, Face recognition from range data by structural analysis, in *Syntactic and Structural Pattern Recognition,* (G. Ferraté, *et al.*, Eds.), Springer-Verlag, New York/Berlin, 1988.
31. M. Turk and A. Pentland, Representing faces for recognition, *Vision Sci. Tech. Rep. 132,* MIT Media Lab., 1990.

32. I. Craw, H. Ellis, and J. R. Lishman, Automatic extraction of face-features, *Pattern Recognition Lett.* **5**, 1987, 183–187.
33. D. Paglieroni, *Control Point Algorithms for Contour Processing and Shape Analysis*, Ph.D. thesis, University of California at Davis, 1986.
34. R. Bartels, J. Beatty, and B. Barsky, *An Introduction to Splines for Use in Computer Graphics and Geometric Modeling*, Kaufmann, Los Altos, CA, 1987.
35. S. C. Eisenstat, H. C. Elman, and M. H. Schultz, Variational Iterative Methods for nonsymmetric systems of linear equations, *SIAM J. Numer. Anal.* **20**, 1983, 345–357.

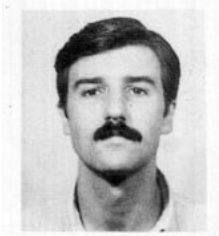

GUILLERMO A. BARICCO received the diploma degree in Computer Sciences from the University of Buenos Aires in 1992. Since 1990 he has been working with the Computer Research and Advanced Applications Group (CRAAG), IBM Argentina. His research interests are in the areas of pattern recognition and machine vision applications.

ALFREDO OLIVERO graduated from the Escuela Superior Latino Americana de Informatica, Argentina, in 1991. During 1990 and 1991 he was a Resident Researcher at the Computer Research and Advanced Applications Group in IBM Argentina. Since 1992, he has been a Ph.D. student at the Institut National Polytechnique de Grenoble, France. His research interests include development of tools for designing and verifying real-time systems.

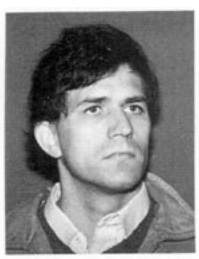

EDUARDO J. RODRÍGUEZ received the degree of Licenciado en Informatica from ESLAI (Escuela Superior Latino Americana de Informatica), Argentina. Since 1990, he has been a Resident Researcher at the Computer Research and Advanced Applications Group, IBM Argentina. He has also been a Visiting Researcher at IBM Almaden Research Center, San Jose, CA. His current areas of interest are computer aided geometric modeling and statistical pattern recognition as applied to image processing.

FELIX G. SAFAR received the Telecommunications Engineer degree in 1980 from the National University of La Plata, Argentina, and the M.S.E.E. degree in 1988 from Virginia Polytechnic Institute and State University, Blacksburg, VA.

He has been a Research Assistant during the years 1980–1985 and a Research Associate since 1985 for the National Science and Technical Research Council (CONICET) of Argentina. Since 1986 he has also been working as an Adjoint Professor at the Informatics Department of the National University of La Plata. In 1990 he joined IBM Argentina and began working as a consultant for CRAAG (Computer Research and Advanced Applications Group). His teaching, research, and consulting interests include signal and image processing, computer vision, information theory, and computer architecture.

Engineer Safar is a Rotary International Scholar and a member of the Phi Kappa Phi honor society.

JORGE SANZ received Master's degrees in computer science in 1977 and in mathematics in 1978, both from the University of Buenos Aires. In 1981 he obtained his Ph.D. in applied mathematics, working on the complexity of algorithms, from the same university. He has been the recipient of many scholarships. Dr. Sanz has been a research staff member in the Computer Science Department, IBM Research Laboratory, San Jose, California from 1984 to 1993. He is now with the Electrical and Computer Engineering Department of the University of Illinois at Urbana–Champaign as a full professor. He conducts research on industrial machine vision, parallel computing, and multidimensional signal processing. Dr. Sanz was technical manager of the machine vision group during the years 1985–1986. Since 1985, he has also been an adjunct associate professor with the University of California at Davis, where he conducted research as the Associate Director of the Computer Vision Research Laboratory until 1988. Dr. Sanz has also served as a consultant for several companies in the United States. Dr. Sanz is the chairman of the Industrial Machine Vision Chapter of the International Association of Pattern Recognition and a member of the Architecture Chapter of the same organization. He is a fellow member of the IEEE, a committee member of the Multidimensional Signal Processing Group of the IEEE Acoustic, Speech, and Signal Processing Society, a member of the Argentinean Institute of Mathematics, and a member of ACM. Dr. Sanz's areas of broad professional interest are computer science and applied mathematics. Specifically, he is interested in multidimensional signal and image processing, image analysis, machine vision, parallel processing, numerical analysis, and computer architectures.